

Structure—Properties Relationships for Manganese Perovskites

B. Dabrowski, X. Xiong, O. Chmaissem, Z. Bukowski
Department of Physics, Northern Illinois University, DeKalb, IL 60115

J. D. Jorgensen
Materials Science Division, Argonne National Laboratory, Argonne, IL 60439

To Be submitted to the International Conference on Superconductors and Magnetic Materials
and Research Technologies, SMART 1999, September 18-23, Hyeres, France.

The submitted manuscript has been created by the University of Chicago as Operator of Argonne National Laboratory ("Argonne") under Contract No. W-31-109-ENG-38 with the U.S. Department of Energy. The U.S. Government retains for itself, and others acting on its behalf, a paid-up, nonexclusive, irrevocable worldwide license in said article to reproduce, prepare derivative works, distribute copies to the public, and perform publicly and display publicly, by or on behalf of the Government.

RECEIVED
JAN 18 2000
OSTI

This work was supported by the U.S. Department of Energy under contract W-31-109-ENG-38 and work at NIU was supported by the ARPA/ONR and the State of Illinois under HECA.

DISCLAIMER

This report was prepared as an account of work sponsored by an agency of the United States Government. Neither the United States Government nor any agency thereof, nor any of their employees, make any warranty, express or implied, or assumes any legal liability or responsibility for the accuracy, completeness, or usefulness of any information, apparatus, product, or process disclosed, or represents that its use would not infringe privately owned rights. Reference herein to any specific commercial product, process, or service by trade name, trademark, manufacturer, or otherwise does not necessarily constitute or imply its endorsement, recommendation, or favoring by the United States Government or any agency thereof. The views and opinions of authors expressed herein do not necessarily state or reflect those of the United States Government or any agency thereof.

DISCLAIMER

Portions of this document may be illegible in electronic image products. Images are produced from the best available original document.

Structure--Properties Relationships For Manganese Perovskites

B. Dabrowski, X. Xiong, O. Chmaissem, Z. Bukowski,
Department of Physics, Northern Illinois University, DeKalb, IL 60115

J.D. Jorgensen,
Materials Science Division, Argonne National Laboratory, Argonne, IL 60439

ABSTRACT

By combining the results of dc magnetization, ac susceptibility, magnetoresistivity, magnetostriction, and x-ray and neutron powder diffraction data for stoichiometric $\text{La}_{1-x}\text{Sr}_x\text{MnO}_3$ we have constructed a phase diagram that describes the magnetic, transport, and structural properties and the relationships among them as a function of composition and temperature. Correlations among physical and structural properties have been observed that are consistent with a competition between ferromagnetism and JT distortion. A metallic state occurs below the Curie temperature when both coherent and incoherent JT distortions are suppressed.

INTRODUCTION

For several decades the $\text{La}_{1-x}\text{A}_x\text{MnO}_3$ ($\text{A} = \text{Sr}, \text{Ba}, \text{Ca}$) compounds have been considered a classical example of materials for which the interactions between electrons are mediated mostly by magnetic super- and double-exchange interactions.[1-3] Recently, increased interest has been generated for these compounds because of a colossal magnetoresistive effect for the ferromagnetic phase ($x \geq 0.1$) near the Curie temperature, $T_C \sim 140 - 380$ K.[4] Renewed theoretical work has shown that the explanation of the transport and magnetic properties requires consideration of electron-phonon couplings in addition to magnetic interactions.[5-7] For LaMnO_3 , a high-spin electronic configuration $t_{2g}^3 e_g^1$ for the Mn^{3+} ions with core-like t_{2g} states and extended e_g orbitals is susceptible to a strong electron-phonon coupling of the Jahn-Teller (JT) type that splits the e_g states into filled d_{z^2} and empty $d_{x^2-y^2}$ orbitals, and, thus, produces large asymmetric oxygen displacements around the Mn ions. The super-exchange interaction that induces ferromagnetic coupling within the Mn-O planes between JT-

ordered orbitals of dissimilar symmetry and antiferromagnetic coupling perpendicular to the planes between orbitals of the same symmetry produces A-type, 3-dimensional antiferromagnetic structure. With substitution of divalent elements for La, electrons are removed from the d_{z^2} orbital causing weakening of both the JT-electron-phonon coupling and the superexchange interaction. Empty states in the e_g orbitals allow for the "breathing-mode" electron-phonon coupling of the charge ordered type that can produce charge localization and a double-exchange ferromagnetic interaction that favors metallic state.[3,8,9]

Competition between magnetic and electron-phonon interactions and structural transitions results in a very rich structure-property phase diagram for substituted LaMnO_3 materials.[10-12] Upon substitution of Sr, $\text{La}_{1-x}\text{Sr}_x\text{MnO}_3$ transforms from an antiferromagnetic insulator to a ferromagnetic insulator at $x \approx 0.1$ and to a ferromagnetic metal at $x \approx 0.16$. The Curie temperature increases from ~ 150 K for $x \approx 0.1$ to ~ 300 K for $x \approx 0.2$, and to ~ 380 K for $x \approx 0.3$. Three crystallographic phases have been identified at room temperature. For pure and lightly substituted materials, the orthorhombic $Pbnm$ structure (O'), characterized by large coherent orbital ordering of the JT-type was found.[10,11,13-16] Above $x \approx 0.08 - 0.12$, a phase (O^*) with the same orthorhombic $Pbnm$ structure but characterized by a considerably smaller coherent JT-orbital ordering is observed.[10,11] At higher Sr substitution level, $x \approx 0.16 - 0.18$, the rhombohedral $R3m$ structure (R), characterized by the absence of a coherent JT orbital ordering, was observed.[10]

The reported values of the compositions and temperatures for the structural, magnetic and resistive transitions vary substantially in the literature, depending on the sample processing method and synthesis conditions.[17] The discrepancies among existing phase diagrams may result from comparing behavior of compositions that are incorrectly assumed to have the same doping level.[18,19] We have recently shown that there can be large deviations from nominal stoichiometry for low and moderate substitution levels ($0 \leq x \leq 0.3$) - the perovskite structure can form a large concentration of vacancies, v , on both the La and Mn sites during synthesis under oxidizing conditions. Since the physical and structural properties are complex and are very sensitive to the hole concentration, we have established the intrinsic phase diagram

(see Fig. 4) as a function of the hole doping; i.e., as a function of the Sr substitution level for samples that contain no metal-site vacancies ($v \approx 0$). [20-22]

SAMPLE PREPARATION AND CHARACTERIZATION

Polycrystalline samples of $\text{La}_{1-x}\text{Sr}_x\text{MnO}_3$ with $0.1 \leq x \leq 0.2$ and $\Delta x = 0.005$, were synthesized using a wet-chemistry method that leads to homogenous mixing of the metal ions. The final firing temperatures and oxygen atmosphere as well as holding times and cooling rates for obtaining stoichiometric samples were determined from TGA measurements performed using slow heating (2 deg/ min.) and cooling (0.6 deg/ min.) rates. Figure 1 shows the oxygen contents from TGA data for a sample with $x = 0.185$. The materials obtained after slow cooling in 100 and 20 % O_2 have the effective oxygen contents substantially above 3. Using the measured oxygen contents shown on Fig.1, the vacancy concentrations of these samples can be estimated (assuming equal amounts on both metal sites) as $v \approx d/(d+3)$. The weights of the samples approached stable levels, indicating a stoichiometric oxygen content of 3.002 ± 0.002 for temperatures around 1360 C. Stoichiometric $\text{La}_{1-x}\text{Sr}_x\text{MnO}_3$ samples were prepared in air by quenching from high temperatures, 1450 C for $x = 0.10$, and gradually lower temperatures for samples with larger x , to 1350 C for $x = 0.20$. Powder x-ray diffraction at room temperature confirmed single-phase material in each case and was used to determine structural phase boundaries. The $x = 0.10$ sample is orthorhombic- O' and a transition from the orthorhombic O' to the O^* structure occurs around $x = 0.11$. The $x = 0.115$ composition is mixed phase, mostly O^* . Compositions from $x = 0.12$ to 0.165 are pure orthorhombic O^* . A transition from the orthorhombic O^* phase to rhombohedral phase occurs for the $x = 0.17$ composition. Above $x = 0.17$, samples are rhombohedral.

PROPERTIES OF $\text{La}_{0.835}\text{Sr}_{0.165}\text{MnO}_3$

We have constructed the structure-properties phase diagram by combining the results of physical property and structural measurements. The magnetic and structural phase transitions were found to exhibit distinctive signatures in each kind of measurement. In Fig. 2 is shown magnetization and resistivity data for an $x = 0.165$ sample for which the ferromagnetic transition appears in the orthorhombic O^* structure. Two features are seen in the magnetic data (Fig. 2a): The clearly visible ferromagnetic

transition at $T_c = 256$ K and the less apparent decreased-magnetization anomaly at $T_s = 125$ K. Both transitions can be precisely defined for small magnetic fields (~ 20 Oe) from the largest slope of the $M(T)$ curves. These magnetic transitions are clearly correlated with the resistive transitions (Fig. 2b), the sharp drop of resistivity at T_c , and the metal-insulator transition at T_s . In addition, the resistivity and ac susceptibility have shown anomalies at $T_f = 310$ K that correspond to the rhombohedral-orthorhombic (R-O*) structural transition. Magnetization and resistivity data obtained for other $\text{La}_{1-x}\text{Sr}_x\text{MnO}_3$ samples showed similar transitions at consistently changing temperatures allowing the correlated transport, magnetic, and structural phenomena to be characterized for each kind of phase transition that occurs in this system.

The neutron diffraction technique was used to accurately determine bond lengths, bond angles, and incoherent oxygen displacements. The pattern of the coherent displacements and the symmetry of the incoherent displacements have been used to obtain information about polaronic electron-phonon interactions in both the paramagnetic and ferromagnetic phases. Figure 3 shows the Mn-O bond lengths and the anisotropic Debye-Waller parameters for $\text{La}_{0.835}\text{Sr}_{0.165}\text{MnO}_3$. The sample is rhombohedral at high temperature, 340 K, and all Mn-O bonds are of equal length; i.e., there is (by symmetry) no coherent JT distortion for this phase. The Debye-Waller parameter is isotropic with magnitude that indicates the presence of incoherently distorted Mn-O_6 octahedra. On cooling below 340 K, the rhombohedral structure changes to orthorhombic O* with a small coherent JT distortion, ~ 0.01 Å. The average bond length increases significantly. These structural changes are consistent with increased resistivity at $T \sim 312$ K in the paramagnetic phase upon the transition from the rhombohedral to O* phase. On further cooling, an abrupt decrease of the lattice parameters appears at the ferromagnetic transition temperature $T_c \sim 256$ K. The individual Mn-O bond lengths do not show clear drops below T_c and the coherent Jahn-Teller distortion remains practically unchanged. However, below T_c , the average Mn-O bond length shows a slight decrease, ~ 0.003 Å. Simultaneously, the average bond angle displays a slight increase, ~ 0.4 degrees. The incoherent JT distortion along the Mn-O bond shows a slight decrease. The sharp drops of resistivity at the ferromagnetic transition can be explained, thus, as resulting from removal of charge localization below T_c by a strong electron-phonon JT-coupling and a narrowing of the band-width in

addition to removal of the spin scattering by double-exchange. On cooling below ~ 160 K, an additional structural change takes place in the ferromagnetic phase. The temperature range of this structural change correlates very well with the resistive and magnetic anomalies which can be clearly identified with the vestiges of the structural O^* to O' change. The equatorial bonds show an abrupt change that indicates an increase of the coherent JT distortion from ~ 0.01 to ~ 0.03 Å. All these changes are consistent with the O^* to O' transition that is suppressed in the ferromagnetic state. The average bond-length shows a slight increase and the average bond angle displays a slight decrease on cooling. These changes are, again, consistent with the more insulating bonds in the O' phase as seen by the metal-insulator resistive transition.

The magnetic structure and its correlation with the coherent JT distortion have been studied as a function of temperature using neutron powder diffraction, magnetoresistance, and magnetostriction. A correlation between the ferromagnetic spin orientation and the coherent JT distortion was observed, indicating a coupling between the structural and magnetic properties. Fig.3(c) shows the refined spin angle ϕ with respect to the crystallographic c -axis. For the $\text{La}_{0.835}\text{Sr}_{0.165}\text{MnO}_3$ sample one can observe simultaneous transitions for both the spin orientation and the coherent JT distortion. Above 160 K, where the coherent JT distortion is very small, the refined spin angle, ϕ , is $\sim 18^\circ$. The spin angle jumps to 40° at 120 K and remains at this value to the lowest temperature, while the JT distortion reaches its maximum value at ~ 120 K and remains constant to the lowest temperature. The magnetoresistance data have shown that the corresponding metal-insulator transition in the ferromagnetic phase is practically insensitive to applied magnetic field. On the other hand, the temperature of the ferromagnetic transition temperature increases from 256 K at 0 T to 290 K at 7 T. With increasing magnetic field the ferromagnetic transition begins to overlap with the resistive anomaly originating from the structural R/O^* transition in the paramagnetic phase. As a result the resistive anomaly caused by the structural R/O^* transition is clearly suppressed. The magnetostriction measurements are consistent with these observations. For $x = 0.165$, the pronounced minimum at 250 K is clearly observed only at 0 T. At a magnetic field of 5 T the minimum is reduced and broadened and at 10 T it is not observable at the highest temperatures of our measurements (300 K). The

observed large change of magnetostriction indicates considerable changes of the lattice constants during the ferromagnetic transition for the $\text{La}_{0.835}\text{Sr}_{0.165}\text{MnO}_3$ sample with the O^* structure as seen from neutron diffraction.[20] Similar rapid decreases of lattice constants and anisotropic Debay-Waller factors were observed for the $\text{La}_{0.75}\text{Ca}_{0.25}\text{MnO}_3$ sample with O^* structure, and interpreted in terms of removal of the incoherent JT-distortions during the ferromagnetic transition.[23] The broad maximum of magnetoresistance was observed in the temperature range 120 - 135 K to be practically independent of magnetic field. Thus, it appears that when the structural O^*/O' transition occurs in the ferromagnetic phase, no additional structural changes are induced by the external magnetic fields up to 10 T.

PHASE DIAGRAM

Based on similar data obtained for the whole series of samples, the following structure-properties relationships were developed for moderately substituted $\text{La}_{1-x}\text{Sr}_x\text{MnO}_3$. In the high temperature paramagnetic regime three structural phases are present: Orthorhombic Pbnm structure characterized by the large coherent orbital ordering of the JT-type and small incoherent JT-distortions, Orthorhombic Pbnm structure characterized by a small coherent JT-orbital ordering and large incoherent JT-distortions, and Rhombohedral R3m structure characterized by the absence of a coherent JT-orbital ordering and large incoherent JT-distortions. For $0.10 < x < 0.145$, during the ferromagnetic transition, the orthorhombic O' phase changes to an orthorhombic O^* phase characterized by suppressed coherent JT-orbital ordering and large incoherent JT-distortions. For $0.15 < x < 0.17$, on cooling during the ferromagnetic transition the insulating orthorhombic O^* phase changes to a metallic O^* phase characterized by small coherent and small incoherent JT-distortions. Below the Curie temperature, in the ferromagnetic phase, this orthorhombic O^* phase changes to an orthorhombic O^* phase characterized by suppressed coherent JT-orbital ordering and large incoherent JT-distortions that is insulating. For $0.175 < x < 0.20$, on cooling during the ferromagnetic transition the semiconducting R phase changes to a metallic R phase with small incoherent JT-distortions. Below the Curie temperature, in the ferromagnetic phase, this R structure changes to an orthorhombic Pbnm structure O^* characterized by small coherent JT-orbital ordering and small incoherent JT-distortions that is still

metallic. Development of ferromagnetic order, thus, suppresses the coherent JT-distortions for the O' phase and incoherent distortions for the O* and R phases. The arrangement of the spins varies from ferromagnetic ordered mainly along the b-axis ($x = 0.11$) to ferromagnetic almost along the c-axis ($x = 0.185$) in the Pbnm symmetry.

The data clearly show that the ferromagnetic phase has lower resistivity than the paramagnetic phase. However, the ferromagnetic transition is accompanied by structural changes that can also cause a decrease of resistivity. The suppression of coherent JT-distortions lowers the resistivity but is not sufficient to produce a metallic phase unless large incoherent JT-distortions are also removed. The electron-phonon Jahn-Teller interactions and the magnetic super-exchange and double-exchange interactions are of similar strength. These interactions compete for the same e_g electrons and, thus, lead to colossal spin-charge-lattice coupling.

ACKNOWLEDGMENT

The work at NIU was supported by the ARPA/ONR and the State of Illinois under HECA, and at ANL by US DOE (W-31-109-ENG-38)

REFERENCES

1. C. Zener, Phys. Rev. 82, 403 (1951).
2. P.W. Anderson and H. Hasegawa, Phys. Rev. 100, 675 (1955).
3. J.B. Goodenough, *Magnetism and chemical bond*, Wiley, New York, 1963.
4. R.M. Kusters, J. Singelton, D.A. Keen, R. McGreevy, and W. Hayes, Physica B 155, 362 (1989).
5. A.J. Millis, P.B. Littlewood, and B.I. Shraiman, Phys. Rev. Lett. 74, 5144 (1995).
6. A.J. Millis, B.I. Shraiman, and R. Mueller, Phys. Rev. Lett. 77, 175 (1996).
7. H. Roder, J. Zhang, and A.R. Bishop, Phys. Rev. Lett. 76, 1356 (1996).
8. P.A. Cox, *Transition Metal Oxides*, Clarendon Press, Oxford, 1995.
9. G.H. Jonker and J.H. Van Santen, Physica 16, 337 (1950).
10. A. Urushibara, Y. Moritomo, T. Arima, A. Asamitsu, G. Kido, Y. Tokura, Phys. Rev. B 51, 14103 (1995).
11. H. Kawano, R. Kajimoto, and H. Yoshizawa, Phys. Rev. B 53, R14709 (1996).
12. J.-S. Zhou, J.B. Goodenough, A. Asamitsu, and Y. Tokura, Phys. Rev. Lett. 79, 3234 (1997).
13. E.O. Wollan and W.C. Koehler, Phys. Rev. 100, 545 (1955).
14. J.B.A.A. Elemans, B. Van Laar, K.R. Van Der Veen, and B.O. Loopstra, J. Solid State Chem. 3, 238 (1971).
15. Q. Huang, A. Santoro, J.W. Lynn, R.W. Erwin, J.A. Borchers, J.L. Peng, and R.L. Greene, Phys. Rev. B 55, 14987 (1997).
16. J. Rodriguez-Carvajal, M. Hennion, F. Moussa, A.H. Moudden, L. Pinsard, and A. Revcolevschi, Phys. Rev. B 57, R3189 (1998).
17. J.F. Mitchell, D.N. Argyriou, C.D. Potter, D.G. Hinks, J.D. Jorgensen, and S.D. Bader, Phys. Rev. B 54, 6172 (1996).
18. J.A.M. Van Roosmalen, and E.H.P. Cordfunke, J. Solid State Chem. 110, 106 (1994).
19. B. Dabrowski, K. Rogacki, X. Xiong, P.W. Klamut, R. Dybziński, J. Shaffer, and J.D. Jorgensen, Phys. Rev. B 58, 2716 (1998).
20. B. Dabrowski, X. Xiong, Z. Bukowski, R. Dybziński, P.W. Klamut, J.E. Siewenie, O. Chmaissem, J. Shaffer, C.W. Kimball, J.D. Jorgensen, Phys. Rev. B
21. X. Xiong, B. Dabrowski, O. Chmaissem, Z. Bukowski, S. Kolesnik, R. Dybziński, C.W. Kimball, J.D. Jorgensen Phys. Rev. B
22. B. Dabrowski, L. Gladczuk, A. Wisniewski, Z. Bukowski, R. Dybziński, A. Szewczyk, M. Gutowska, S. Kolesnik, C.W. Kimball, and H. Szymczak (unpublished)
23. P.G. Radaelli, G. Iannone, M. Marezio, H.Y. Hwang, S-W. Cheong, J.D. Jorgensen and D.N. Argyriou, Phys. Rev. B 56, 8265 (1997).

FIGURE CAPTIONS

Fig. 1 Oxygen contents in 1, 20, and 100 % O₂ from thermogravimetric measurements for La_{0.835}Sr_{0.165}MnO_{3+d} sample. The data were obtained during slow cooling at 0.6 deg/min.

Fig. 2 Magnetization in a 20 Oe applied field (a) and resistivity (b) and for the La_{0.835}Sr_{0.165}MnO₃ sample.

Fig. 3 Refined structural and magnetic parameters from neutron powder diffraction measurements as a function of temperature for La_{0.835}Sr_{0.165}MnO₃ sample: (a) Mn-O bond lengths and their average value, (b) anisotropic Debye-Waller factors perpendicular and parallel to Mn-O bond, and (c) spin angle with respect to crystallographic c-axis.

Fig. 4 Phase diagram summarizing the magnetic and structural properties of La_{1-x}Sr_xMnO₃ as a function of composition, $0.10 \leq x \leq 0.2$, and temperature, $12 \leq T \leq 350$ K. O*, O', O'', and R stand for the small coherent JT-distorted orthorhombic ($\sigma_{JT} \sim 0.004$ Å), large coherent JT-distorted orthorhombic ($\sigma_{JT} \sim 0.05$ Å), suppressed coherent JT-distorted orthorhombic ($\sigma_{JT} \sim 0.02$ Å), and the rhombohedral phases, respectively.

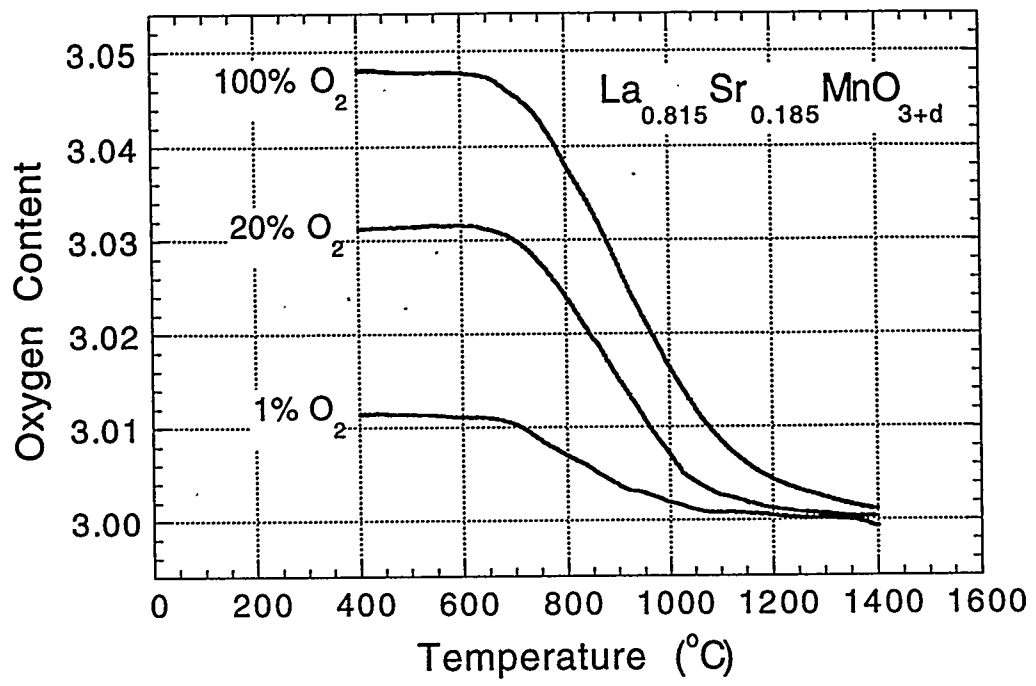


Fig. 4

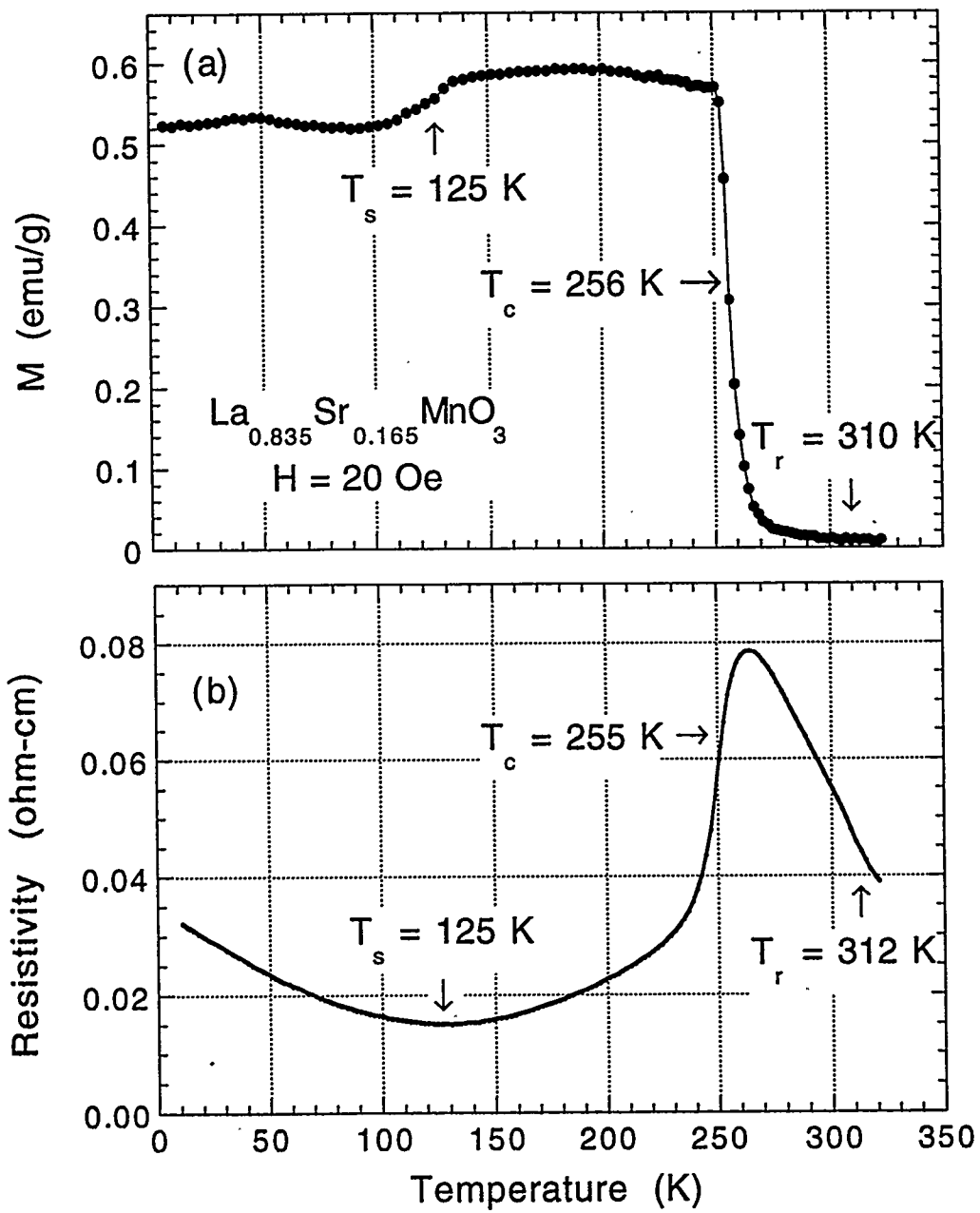


Fig. 2

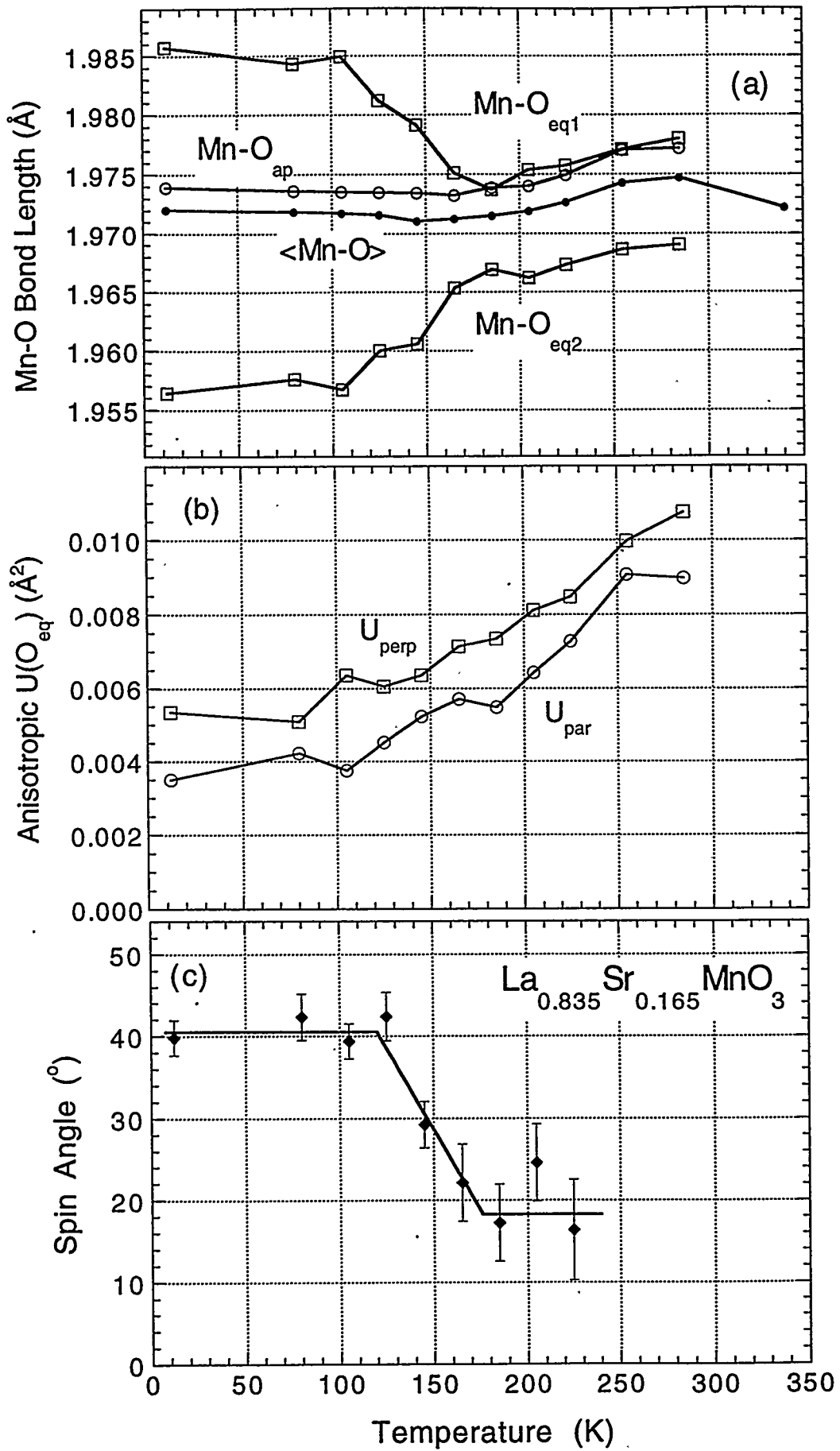


Fig. 3

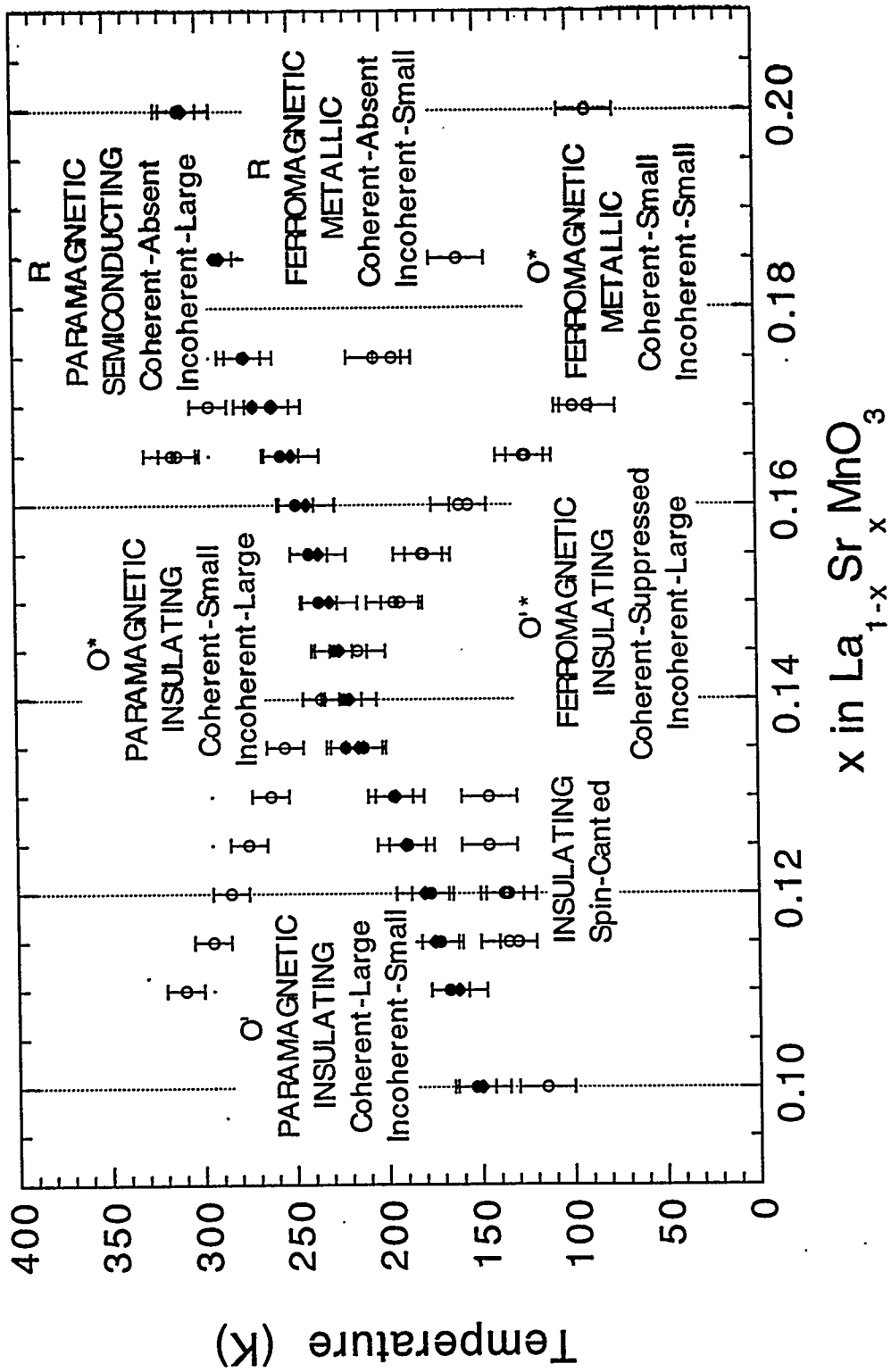


Fig. 4